Assessment of Coronary Microcirculation with High Frame-Rate Contrast-Enhanced Echocardiography

Wahyulaksana, Geraldi; Wei, Luxi; Voorneveld, Jason; te Lintel Hekkert, Maaike; Bowen, Daniel J.; Strachinaru, Mihai; Duncker, Dirk J.; van der Steen, Antonius F.W.; Vos, Hendrik J.

DOI
10.1016/j.ultrasmedbio.2024.12.002

Publication date
2025

Document Version
Final published version

Published in
Ultrasound in Medicine and Biology

Citation (APA)
Wahyulaksana, G., Wei, L., Voorneveld, J., te Lintel Hekkert, M., Bowen, D. J., Strachinaru, M., Duncker, D. J., van der Steen, A. F. W., & Vos, H. J. (2025). Assessment of Coronary Microcirculation with High Frame-Rate Contrast-Enhanced Echocardiography. *Ultrasound in Medicine and Biology*, *51*(3), 585-591. https://doi.org/10.1016/j.ultrasmedbio.2024.12.002

Ultrasound in Medicine & Biology 51 (2025) 585–591

Contents lists available at ScienceDirect

Ultrasound in Medicine & Biology

journal homepage: www.elsevier.com/locate/ultrasmedbio

Original Contribution

Assessment of Coronary Microcirculation with High Frame-Rate Contrast-Enhanced Echocardiography

Geraldi Wahyulaksana [a,b], Luxi Wei [a], Jason Voorneveld [a], Maaike te Lintel Hekkert [c], Daniel J. Bowen [d], Mihai Strachinaru [a,d], Dirk J. Duncker [c], Antonius F.W. van der Steen [a,e], Hendrik J. Vos [a,e,*]

[a] Biomedical Engineering, Cardiology, Erasmus MC University Medical Center Rotterdam, Rotterdam, The Netherlands
[b] Department of Radiology, Weill Cornell Medicine, NY, USA
[c] Experimental Cardiology, Cardiology, Erasmus MC University Medical Center Rotterdam, Rotterdam, The Netherlands
[d] Cardiology, Erasmus MC University Medical Center Rotterdam, Rotterdam, The Netherlands
[e] Medical Imaging, Department of Imaging Physics, Faculty of Applied Sciences, Delft University of Technology, Delft, the Netherlands

ARTICLE INFO

Keywords:
Echocardiography
Echography
Contrast-enhanced
High frame rate
In vivo
Coronary vasculature
Blood perfusion
Higher order singular value decomposition

ABSTRACT

Objective: Assessing myocardial perfusion in acute myocardial infarction is important for guiding clinicians in choosing appropriate treatment strategies. Echocardiography can be used due to its direct feedback and bedside nature, but it currently faces image quality issues and an inability to differentiate coronary macro- from micro-circulation. We previously developed an imaging scheme using high frame-rate contrast-enhanced ultrasound (HFR CEUS) with higher order singular value decomposition (HOSVD) that provides dynamic perfusion and vascular flow visualization. In this study, we aim to show the ability of this technique to image perfusion deficits and investigate the potential occurrence of false-positive contrast detection.

Methods: We used a porcine model comprising occlusion and release of the left anterior descending coronary artery. During slow contrast agent infusion, the afore-mentioned imaging scheme was used to capture and process the data offline using HOSVD.

Results: Fast and slow coronary flow was successfully differentiated, presumably representing the different compartments of the micro-circulation. Low perfusion was seen in the area that was affected, as expected by vascular occlusion. Furthermore, we also imaged coronary flow dynamics before, during and after release of the occlusion, the latter showing hyperemia as expected. A contrast agent destruction test showed that the processed images contained actual contrast signal in the cardiac phases with minimal motion. With larger tissue motion, tissue signal leaked into the contrast-enhanced images.

Conclusion: Our results demonstrate the feasibility of HFR CEUS with HOSVD as a viable option for assessing myocardial perfusion. Flow dynamics were resolved, which potentially helped to directly evaluate coronary flow deficits.

Introduction

ST-segment elevation myocardial infarction is a critical type of coronary artery disease caused by complete blockage of a major coronary artery and is associated with high morbidity and mortality [1]. Primary percutaneous coronary intervention (PCI) within 120 min of symptom onset is the preferred treatment for acute ST-segment elevation myocardial infarction, with a high success rate in re-opening blocked vessels [1,2]. However, despite successful image-proven flow restoration within the epicardial major coronary arteries, up to 60% of patients show suboptimal reperfusion in the microcirculation, known as the 'no-reflow' (NR) phenomenon. The pathophysiological mechanism of NR is complex and still not completely understood [3,4]. Nonetheless, the occurrence of NR after PCI is a critical indicator of poor prognosis [5–7]. Distinguishing between different vascular compartments in the coronary microcirculation may aid in further understanding NR. The coronary microcirculation can be divided into arterial and venous compartments. The arterial system consists of pre-arterioles as an intermediate compartment (diameter ~100–500 μm) and a distal compartment (diameter <100 μm) that comprises arterioles and capillaries [8]. The venous microcirculatory compartment consists of venules with an inner diameter below 300 μm [8,9]. The arteriolar distal compartment is where metabolic regulation of myocardial blood flow occurs. Reduced arteriolar function as well as structural remodeling are termed coronary

* Corresponding author. Department of cardiology, Erasmus MC university medical center, PO BOX 2040, 3000-CA Rotterdam, Zuid-Holland, the Netherlands.
E-mail address: H.Vos@ErasmusMC.nl (H.J. Vos).

https://doi.org/10.1016/j.ultrasmedbio.2024.12.002
Received 12 January 2024; Revised 3 December 2024; Accepted 4 December 2024

microvascular dysfunction [8,10], which may play a distinct role in the NR phenomenon. Therefore, it may be beneficial to assess myocardial perfusion through the different compartments during or post myocardial infarction intervention so that clinicians can provide suitable pharmacological treatment, potentially improving patient prognosis [11].

Currently, the standard clinical methods to perform myocardial perfusion imaging include cardiovascular magnetic resonance imaging (CMR), single-photon emission computed tomography (SPECT), positron emission tomography (PET), echocardiography and CT angiography. SPECT is the most commonly used technique but has limited spatial resolution and requires injection of a radioactive tracer. CMR and PET offer good technical capabilities but have limited availability and neither are bedside applicable. Furthermore, SPECT, PET and CT induce ionizing radiation, which could be harmful if performed recurrently [12]. Similarly, CMR uses a gadolinium-based contrast agent that has raised concerns regarding nephrotoxicity [13]. Contrast-enhanced echocardiography, on the other hand, represents a promising option for perfusion assessment as it is non-ionizing and available at the bedside. The ultrasound contrast agent consists of an inert gas-filled microbubble solution that dilutes within the entire cardiovascular system. Microbubble presence in the myocardium indicates perfusion. However, its application in clinical practice has been limited by issues related to reproducibility, variability and general poor image quality [12,14]. Current clinical implementations operate at relatively low frame rates to avoid contrast destruction due to exposure of the contrast agent to imaging pulses, and therefore provide only snap shots without the temporal resolution to show the flow of the contrast agent within the vasculature. This prevents actual imaging of the vascular structure in the myocardium and also lacks discrimination of the different flow compartments that were described above. Moreover, cardiac motion may result in a so-called flash artifact [15], in which tissue signal 'leaks' into the contrast-enhanced images, potentially leading to a false-positive perfusion reading. In modern ultrasound machines, such 'flash' artifacts may be suppressed by image processing, but at the potential cost of also suppressing slowly moving contrast agents within the smaller vasculature.

High frame-rate (HFR) echocardiography is a recent technique in which the echographic machine is programmed to reach at least 10-fold higher frames rates than conventional mode, *i.e.*, approximately 500 frames per second in HFR mode versus approximately 50 frames per second in conventional mode. HFR echocardiography has the potential to enable improved assessment of microvascular flow and the NR phenomenon compared with conventional line-by-line imaging, as the high frame-rate technique can better distinguish between the fast-moving heart wall and various blood flow velocities. A previous study by Maresca et al. [16] demonstrated the possibility of mapping coronary epicardial and pre-arteriole compartments without the use of ultrasound contrast agents using HFR echocardiography. However, use of a linear array probe limited the imaging depth to 3-4 cm, and the larger probe footprint resulted in an unconventional view that was unable to image the entire left ventricular wall due to rib shadowing. Furthermore, the SVD clutter filter [17] that was used could not detect the nearly stationary flow within the arteriole compartment. To improve the sensitivity of echocardiography to detect flow, contrast agents can be injected intravenously. Demeulenaere et al. [18] showed that it is possible to visualize and assess coronary arterioles with HFR contrast-enhanced echocardiography (CEUS). However, they used a small-animal model (rats) where they used high-frequency transmission and pulse repetition frequency to obtain high-quality images not feasible for human application. Studies using HFR CEUS to assess perfusion in a large-animal model, as well as human feasibility demonstration, have been performed by Toulemonde et al. [19,20]. They showed that HFR CEUS was able to continuously obtain contrast signal throughout the cardiac cycle, yet without further discrimination of flow within the coronary microvasculature. In a recent paper [21], a first in-human proof of concept for imaging the vascular structure using HFR imaging and so-called super-localization was presented to visualize the arterial structure within hypertrophic hearts in the diastolic phase, during which limited cardiac motion was present.

We previously developed a novel contrast detection scheme using higher order singular value decomposition (HOSVD) [15,22,23] combined with HFR CEUS that enhances image quality and enables visualization of fast and slow coronary circulation throughout the cardiac phases (systole and diastole) [23]. In the current study, we used a porcine model with induced occlusion of the major coronary artery to assess the technique's ability to detect perfusion deficit and hyperemia, which is pivotal for assessing myocardial infarction and/or microvascular defect. To support discrimination between the two, we applied an earlier technique to differentiate fast and slow flow [23], in which fast flow presumably corresponds to the coronary macro-circulation, pre-arterioles and small coronary veins, and slower flow corresponds to the arterioles, capillaries and venules [24]. Additionally, we used a destruction sequence to rule out false-positive contrast detection in the myocardium. By evaluating the dynamics of myocardial coronary flow throughout the cardiac phases in the occlusion model, we demonstrated the feasibility of HFR CEUS to be a viable option for assessing myocardial perfusion and its deficit.

Methods

Porcine model

A female Yorkshire x Norwegian Landrace pig (38 kg) was used for the experiment, which followed European Union and institutional guidelines for the care and use of laboratory animals; Centrale Commissie Dierproeven approval no. AVD1010020172411 (SP2100125). The animal was first sedated using Zoletil 50 (6 mg/kg), Xylazine (2.25 mg/kg) and Atropine (0.03 mg/kg), then put under full anesthesia using pentobarbital (10–15 mg/kg/h), intubated and mechanically vented. The animal was positioned in a supine position with vital signs monitored. Two more pigs of similar weight received the same treatment, leading to the results presented in Supplementary Figure 1.

A diluted (1:30; *i.e.*, containing a maximum of 4×10^8 microspheres per ml) Definity solution (Lantheus Medical Imaging Inc., MA, USA) was continuously infused through the jugular vein at 1.5 ml/min. The acquisitions were performed by direct cardiac access after sternotomy, where a water-filled plastic bag was used to ensure sufficient acoustic contact between the probe and heart; the resulting stand-off was a few millimeters. A Sprinter over-the-wire balloon dilatation catheter (Medtronic Inc., MN, USA) was placed in the proximal part of the left anterior descending coronary artery right after the first secondary branch, such that the heart would still beat during occlusion (for ethical considerations), yet maintaining a sufficiently large non-perfused area. Angiography was used to verify the catheter location and as a reference for monitoring the occlusion (Fig. 1a, 1b). Additionally, a clinical scanner (Zonare ZS3, P7-3 probe, Mindray Innovation Center, CA, USA) was used as a reference for image quality comparison (Fig. 1c, 1d). During the procedure, the left anterior descending artery (LAD) was transiently occluded by inflating the balloon for 4 min. HFR CEUS acquisitions were performed before, during and after release of the occlusion.

HFR ultrasound acquisition and data processing

Data were acquired using a phased-array P7-4 probe (ATL Philips, Bothell, WA, USA; Fc = 5.2 MHz) connected to a research scanner (Vantage 256 system, Verasonics, WA, USA). As detailed in [23], high frame rate recordings consisted of three overlapping diverging waves that were sequentially transmitted from three non-overlapping sub-apertures (21 elements per sub-aperture) [25], and a three-pulse checkerboard AM sequence was transmitted from each sub-aperture. A frame was built from the nine combinations of the three AM pulses and three sub-

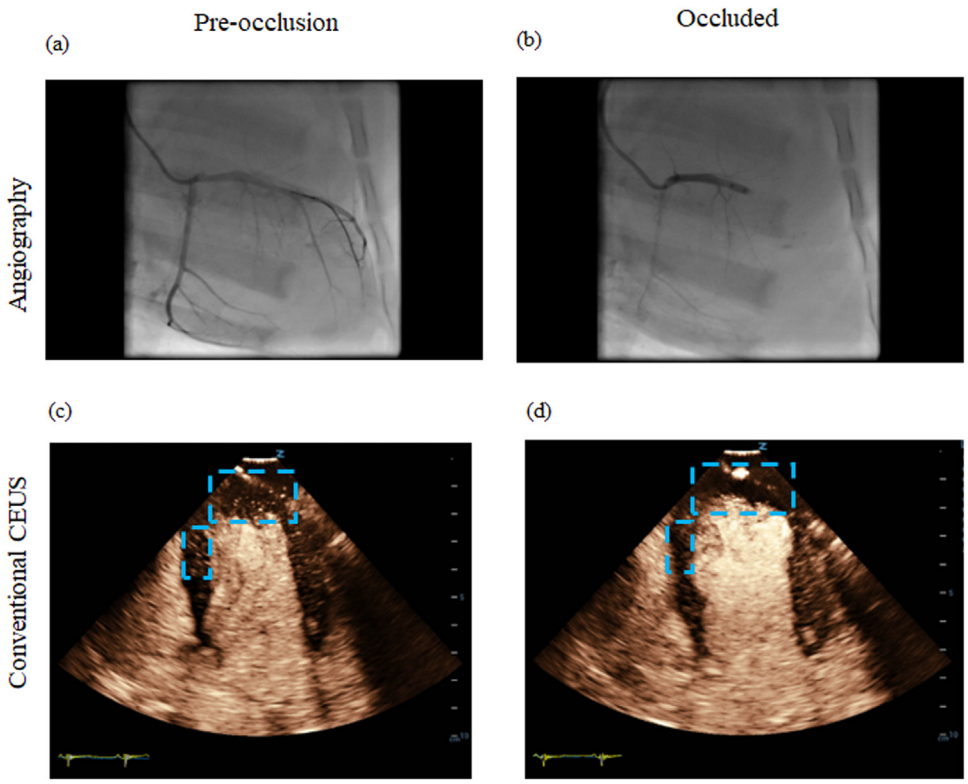

Figure 1. Images acquired by angiography (a, b) and contrast-enhanced echocardiography (c, d) of the left coronary arteries pre- and during occlusion. The apex of the heart, affected by left anterior descending artery occlusion, is marked with cyan boxes.

aperture transmissions; with a pulse repetition frequency of 4.5 kHz, this yielded a final frame rate of 500 Hz. The sequence consisted of 1 s HFR recordings, followed by high-intensity scanning-focused beams for microbubble destruction (21 cycle pulses at 5.2 MHz), and then a subsequent 4 s of repeated HFR recordings. Channel data were beamformed offline using the Ultrasound Toolbox [26] in Matlab (R2022A, 2022; MathWorks, MA, USA) on a 0.5 λ resolution grid. Mechanical index (0.3 dB/cm/MHz derated) values of the imaging and destruction pulses were 0.08 and 0.6 at 5 cm depth, respectively.

We post-processed the data using HOSVD with spatial, temporal and transmit pulses as input dimensions. First, the images from the three sub-apertures were coherently compounded, and then HOSVD was implemented on an ensemble of 20 frames. The *in vivo* spatial rank selection algorithm was implemented based on the gradient of spatial mode singular values using the local peak as a threshold to separate contrast signals from tissue signals, as described earlier [23]. Further, we clustered temporal ranks to distinguish between fast and slow flows in the coronary circulation [23]. Although eigenvectors theoretically contain signals with a range of frequencies from 0 Hz up to the Nyquist frequency, in practice each eigenvector has a dominant range of visible frequencies; *e.g.*, in Figure 8a in [23]. Clustering was done by selecting the HOSVD ranks with a dominant frequency component either above or below 75 Hz. Doppler frequency corresponds to 10 mm/s axial velocity at the used center frequency of 5.2 MHz and speed of sound of 1540 m/s; in practice, by manual tracking we found that approximately half of all detections after 'fast-flow filtering' had a velocity over 10 mm/s, and 90% of detections had a velocity over 5 mm/s. Our assumption was that a flow faster than 10 mm/s was present in the coronary arteries, pre-arterioles and coronary veins, while slower flow was present in the arterioles, capillaries and venules [24]. Data are presented during systole and diastole. Opposite to dominant perfusion characteristics in the rest of the body, myocardial venous flow is expected to be more dominant during systole, and myocardial arterial flow is expected to be dominant during diastole [27].

Results

Images that show pre-occlusion, occluded LAD and post release (hyperemia) scenarios during diastole are shown in Figure 2. In these images, slow and fast-flow representations are superimposed, where the hot colormap represents slow flow (below the frequency cut-off) while grayscale represents fast flow (above the frequency cut-off), presumably corresponding to flow in the arterioles/veins and pre-arterioles, respectively. The occlusion model mostly affects the apex and the upper half of the interventricular septum, as can be seen by the absence of contrast detection in the cyan boxes in Figure 2 when the balloon was inflated to occlude the LAD.

Figure 2 illustrates the effectiveness of our method at detecting vasculature flow and identifying perfusion deficits in the myocardium by visualizing the presence of microbubbles in images when the LAD is open, and their absence when the LAD is occluded. Notable visual distinctions were observed between the pre-occlusion and release phases: After release, coronary fast flow, represented by vessels in grayscale, appeared brighter compared with the pre-occlusion phase, indicating increased microbubble flow in the coronary vessels; this is the so-called 'hyperemia phase' after the release of occlusion that occurs when all vessels are dilated to provide the highest perfusion. Moreover, more microbubbles were detected in smaller vessels, as evidenced by additional red dots in the hot colormap during the release phase compared with the pre-occlusion phase. This supports the capability of our method to detect and visualize flow changes in the microcirculation that are induced by physiological reactions as a result of the occlusion protocol. Supplementary still images from two other animals (Fig. 1S) show similar results.

Figure 3 (also see Supplementary Movie 1S and 2S) depicts the apex of the heart pre-occlusion and after release, and during diastole and systole, including electrocardiogram traces (Fig. 3a, 3b). In the frames the slow and fast flow are shown separately, where a hot colormap represents the slow-flow images (Fig. 3c, 3d, 3g, 3h) and a grayscale colormap

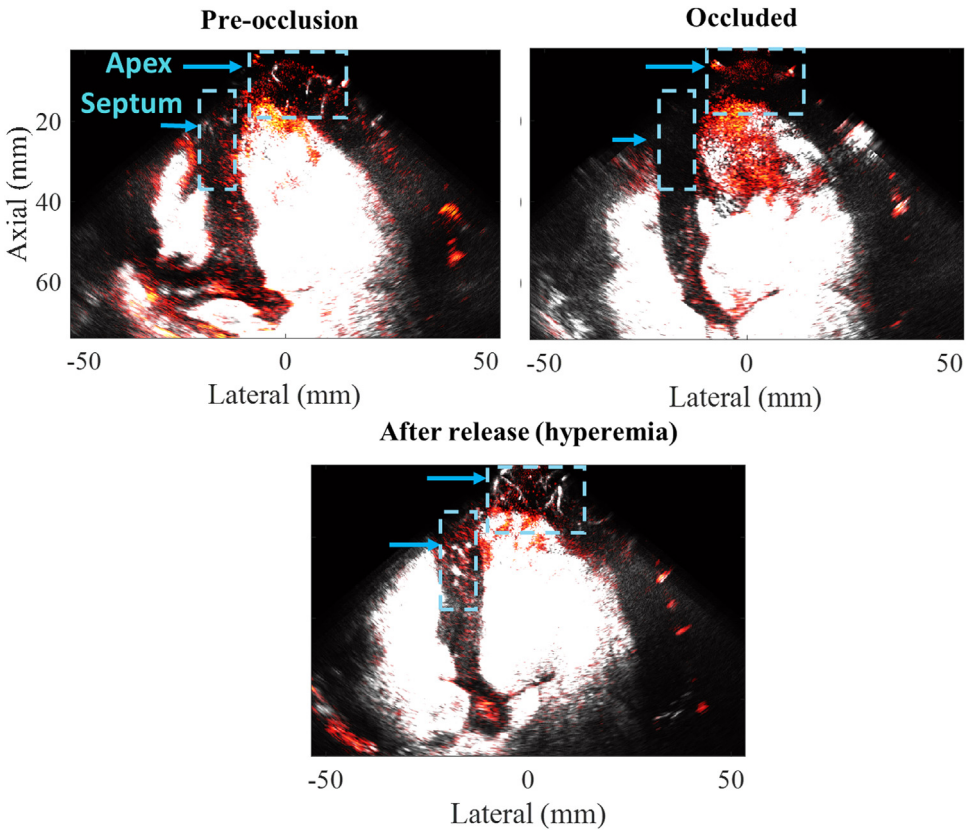

Figure 2. High frame-rate contrast-enhanced echocardiography images in a four-chamber apical view, processed with higher order singular value decomposition pre-occlusion, during occlusion and recordings after release. The apex and interventricular septum of the heart, affected by left anterior descending artery occlusion, are marked with cyan boxes.

represents the fast-flow images (Fig. 3e, 3f, 3i, 3j). Consistent with Figure 2, more microbubbles were detected in the release phase recording compared with the pre-occlusion recording for both cardiac phases and flow speed.

It could be observed that coronary flow is more visible during diastole but not during systole. This is due to myocardial flow being faster during diastole than systole [28]. The flow visualized during different cardiac phases also represents the flow in different coronary vessels, where end-systole is dominated by flow in the veins and diastole is dominated by flow in the arteries [27]. The direction of flow, as shown in the Supplementary movies, also confirms this hypothesis: During end-systole the flow is observed moving upward (toward the apex of the heart), while during diastole it flows downward (from the apex of the heart).

Supplementary Movies 1S and 2S show significant tissue signal leakage during fast cardiac motion, which is visible as a temporary haze over the images. This visual appearance is different from the underlying contrast agent signal as the haze has a larger spatial extent than the single dots and channels that are representative of the contrast signal. The haze was suppressed during low-motion cardiac phases (end-diastole and end-systole), which were therefore used for the still frames in Figure 3 in which the cardiac arterial and venous flow were high and, hence, representative of the microcirculation.

A comparison between pre- and post-destruction sequence images is shown in Figure 4 (see Supplementary Movie 3S for the full recording). These images were acquired while the LAD was occluded, leading to the absence of a microbubble signal in the apex and certain regions. However, in the pre-destruction image both fast- and slow-flow signals were visible in the anterior free wall, which is the perfused part of the myocardium, as highlighted in the cyan box. In this zone no microbubble signal could be detected in the myocardium immediately after destruction, indicating that the signals detected in the myocardium prior to the destruction sequence were indeed from microbubbles. In the post-destruction image, only a fast-flow (grayscale vessel) microbubble signal is visible. The temporary depletion of slow-flow microbubbles (hot colormap) is due to the fact that they need more time to replenish than fast flow, which verifies that the hot colormap signal specifically corresponds to slow-flow microbubbles and not artifacts.

Discussion

Here we have demonstrated that the combination of HFR CEUS and HOSVD is able to visualize slow and fast flow in coronary microcirculation dynamics during cardiac phases, presumably corresponding to flow in the arterioles and pre-arterioles/veins, respectively. Moreover, we were also able to distinguish flow in the arteries and veins based on the direction and velocity of flow during the cardiac phases: inward (arterial) flow during early diastole and outward (venous) flow during early systole. The ability to distinguish between fast and slow flow as well as depicting microvascular structure, capabilities that are not present in current routine clinical echocardiographic modes, increased our confidence in assessing microvasculature obstructions and perfusion deficits. Although few myocardial sectors remain ‘dark’ in the images even if normal perfusion is expected, these sectors are located at larger imaging depths; this difficulty is similar to current perfusion echography standards visible in, for example, the basal part of the septum in Figure 1c. Dark regions of the lateral wall were possibly as a result of loss of sensitivity with the adoption of diverging waves. While the septum is close to the center of the diverging wave beam, the lateral wall is located near the edge of the beam spread, where sensitivity is decreased and not covered by multiple over-lapping beams. This issue may be circumvented by extending the number of cardiac views during examination, such that the cardiac sectors are always imaged from several directions and image depths (A4Ch, A3CH, A2CH, PLAX, PSAX at apical, mid and basal levels).

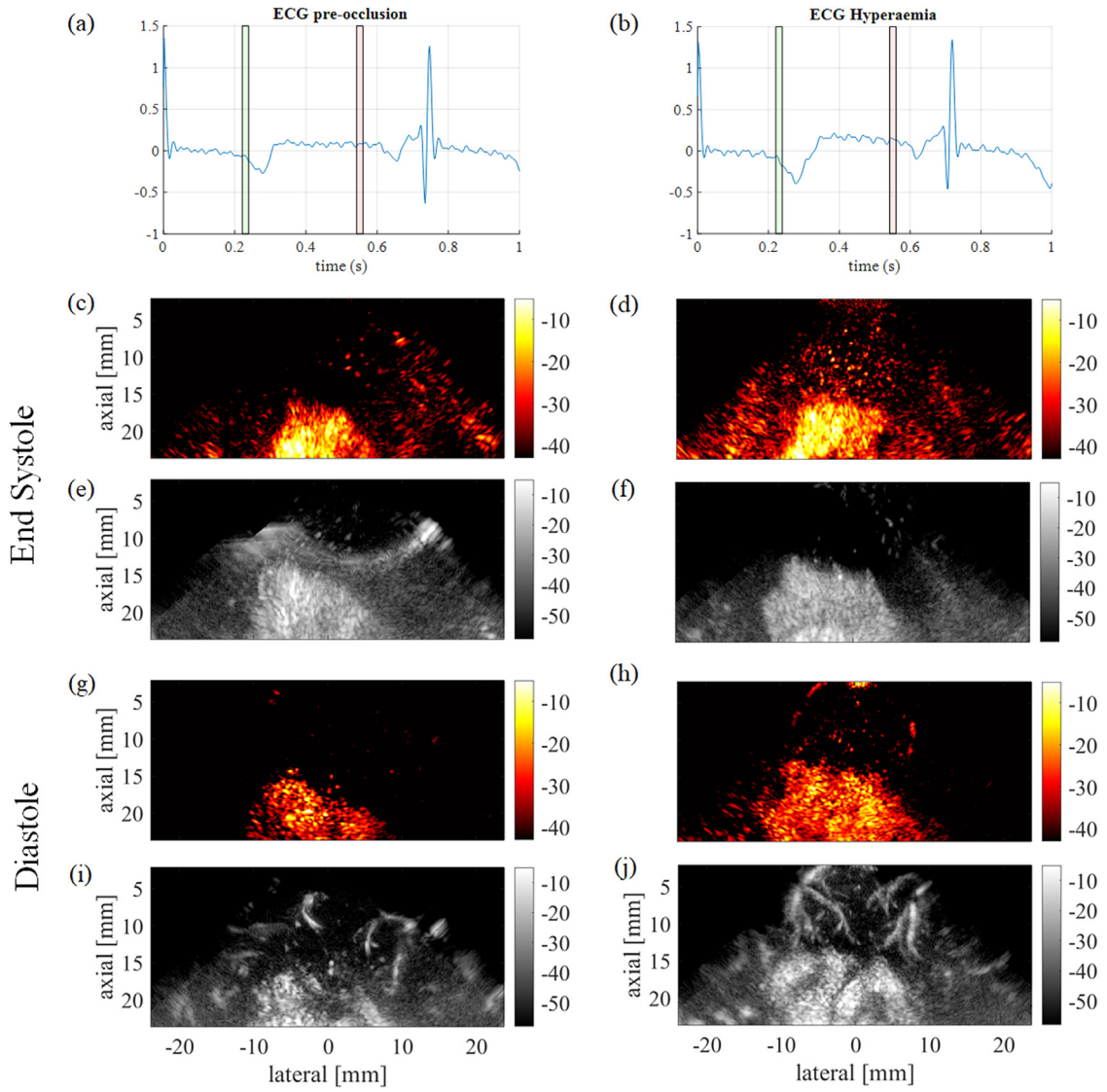

Figure 3. Images acquired by high frame-rate contrast echocardiography pre- and post-occlusion in end-systole and diastole. (a, b) show electrocardiograms of the two acquisitions, where green and red areas represent the period of end-systole and diastole, respectively. Images processed with slow-flow higher order singular value decomposition (HOSVD) are displayed using a hot colormap (c, d, g, h) and fast-flow HOSVD are displayed using a grayscale colormap (e, f, i, j).

Moreover, our study showed the ability of HFR CEUS to accurately visualize regions affected by the occlusion of a major coronary vessel and to display flow dynamic changes resulting from this occlusion model. After release of the occlusion, the images clearly exhibited hyperemia in the LAD area when compared with pre-occlusion images, highlighting the effectiveness of our approach. To validate that the detected signal in the myocardium was indeed microbubble signal and to confirm that the different colormap indeed represented different flow velocities, we showed the absence of contrast signal after a contrast destruction sequence and measured flow velocities.

Our study demonstrates several improvements over previous myocardial perfusion studies that utilized HFR echocardiography. The combination of contrast detection pulses and HOSVD successfully revealed slow and almost stationary flow, presumably in the arterioles, capillaries and venules compartments of the microvasculature, which would remain below the detection threshold of non-contrast sequences due to limitations of the standard SVD filter [16]. Additionally, the use of a phased-array probe as opposed to the linear array probe used earlier for microvascular imaging [16] allowed us to potentially obtain conventional views (apical and parasternal) at an adequate imaging depth, even trans-thoracically. Demeulenaere et al. [18] obtained superior image quality in a small-animal set-up that allowed higher ultrasound frequencies and hence better image quality, but the benefits of having a higher ultrasound frequency were not clinically translatable. When compared to the large-animal study conducted by Toulemonde et al. [19], our HFR CEUS approach provided somewhat superior image quality during the cardiac phase with larger tissue motion, which can be explained by the HOSVD filtering being able to suppress the flash artifact upon mild axial tissue motion [23]. A recent paper by the same group showed that contemporary adult phased-array probes could collect contrast-enhanced high frame-rate vascular data in a proof-of-concept study in adult patients [21].

The ‘flash’ artifact, caused by tissue motion that gives incoherent tissue echo data in most conventional contrast-enhancing pulsing schemes, was observed in both conventionally AM-processed data and HOSVD-processed data, although HOSVD processing was able to reduce the effect [23]. In principle, compounding data from sub-aperture transmissions may also enhance the flash artifact, as compounding reduces the effective frame rate. However, we designed the pulse sequence such that the three-pulse AM ‘checkerboard’ pulse was first transmitted from one of the three sub-apertures before the next sub-aperture was selected for the next AM pulsing triplet. This ensured that the effective pulse repetition intervals for AM pulsing—and hence, the flash artifact—was

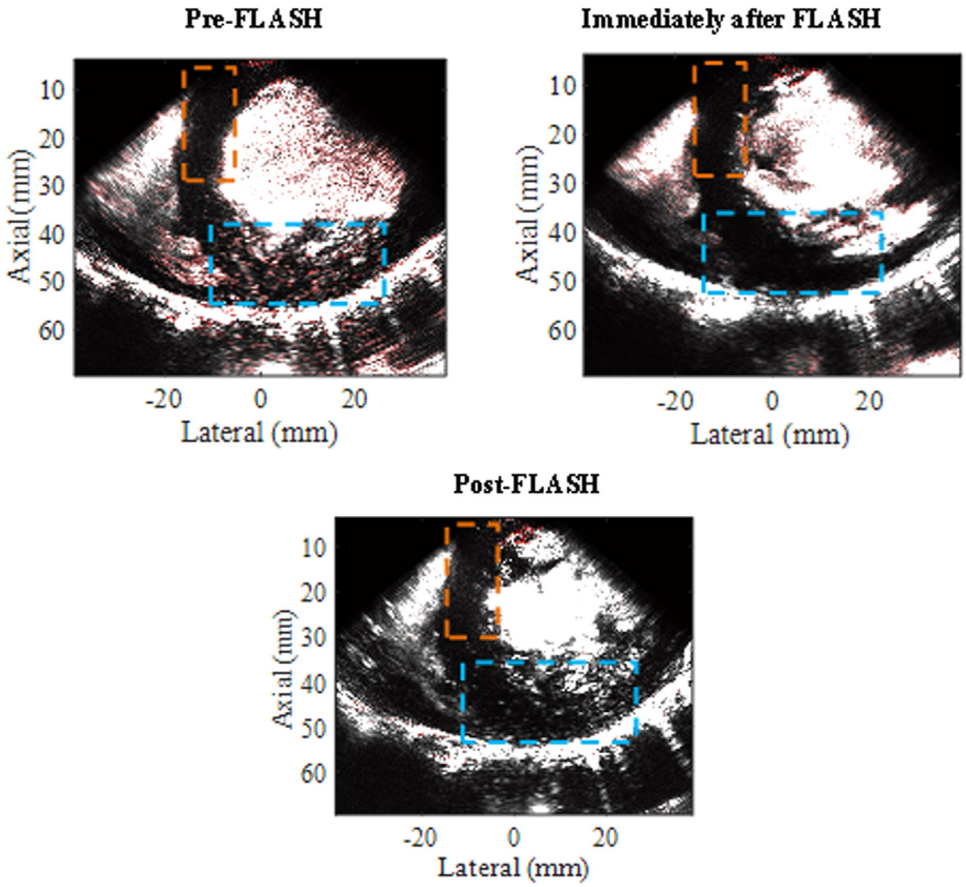

Figure 4. High frame-rate contrast-enhanced echocardiography images in a short-axis parasternal view during occlusion at a time instance of pre-destruction, immediately after the destruction pulses, and two cardiac cycles later. The interventricular septum that is affected by the occlusion is marked by orange boxes. The inferior wall that is not affected by the occlusion is indicated by cyan boxes; vessels with fast flow appear two heart beats after destruction, while the overall perfusion signal has yet to be restored.

minimized at the cost of potentially lower coherency upon compounding the data from the three sub-apertures. This lower coherency gives lower resolution and lower image contrast in time instances of larger tissue motion. However, in these instances, the flash artifact already prevented accurate contrast detection (see Supplementary Movie 1S), and the lower resolution and lower image contrast played no further role. Tissue acceleration and/or non-rigid tissue displacement could further lead to lower coherence between the sub-aperture frames upon compounding but has a lower, second-order effect on the flash artifact.

There are some limitations in our study that still need to be improved. First, HFR acquisitions were performed directly on the porcine heart after sternotomy. It is easier to obtain good image quality when the imaging target is close to the probe, especially with the diverging wave and relatively high-frequency transmission for cardiac imaging that we employed. With open chest acquisition we also did not experience any aberrations from skin, fat and muscle layers that would otherwise generate imaging artifacts and/or attenuation. In human studies, an adult cardiac probe and related ultrasound frequencies (1.7–4 MHz) may be preferred over the pediatric probe operating at 5.2 MHz that we used. We expect that translation of the HOSVD algorithm and rank selection into a clinical study with an adult cardiac probe [21] would be relatively straightforward, as all of the components in the processing pipeline are translatable to a phased or linear array imaging set-up. The second limitation was inherent problems with 2-D imaging, which comprised reproducibility and out-of-plane motion issues [29]. As 2-D imaging implies that only a slice is sampled, slightly different probe placement may significantly affect the results as it could cause plane misalignment and image different vessels. The adoption of volumetric echocardiography could solve these issues. Third, we were unable to remove all imaging artifacts with HOSVD as motion artifacts persisted (Fig. 3e). Motion compensation techniques could potentially reduce these motion artifacts [30]. Last, we did not validate discrimination of the multiple compartments, nor their flow within, using other imaging or measurement techniques. Although no ground truth measurements are available for imaging and discriminating the various microcirculation compartments [8], imperfect yet perhaps insightful comparison with 3-D angiography, computational flow dynamics or flow wire measurements may provide additional validation of our technique.

Flow velocity in any vessel will range from zero to a maximum value simultaneously. However, given the apparent point spread function width in the image (approximately 300 μm corresponding to one wavelength) and the expected vessel diameters (approximately 500 μm and below), we do not expect that this technique could spatially resolve flow velocity regions within the vessel cross-section. However, fast-flow images show structures that resemble vasculature with expected orientations, flow directions (with respect to timing within the cardiac cycle) and speeds, and slow-flow images show more homogeneous detection of contrast signal and stationary signals. As shown in the results, this technique can also distinguish between arterial and venous flow based on flow direction. Future data processing with super-localization techniques may further quantify flow velocities [21]. However, this only provides indirect proof of detection of the vascular compartment, and more research on correct localization and correlation with, for example, histological proof, may be needed to further build evidence.

The successful translation of our developed techniques for myocardial perfusion assessment using HFR CEUS holds the potential to improve accuracy and reliability in visualizing perfusion during or after PCI. It can provide valuable diagnostic information for assessing the

occurrence of NR after PCI, influencing short and long-term treatment decisions, and optimizing patient outcomes. The capillaries were obstructed or ruptured in the no-reflow zone, in which case flow velocity in the pre-arterioles and arterioles could be expected to be lower than in normal conditions, and fewer or no arterioles could be visible in the NR zone. Moreover, post-infarct hyperemia was clearly visible, which may support assessing the condition of at-risk tissue adjacent to the non-perfused core of the ischemic region and hence could direct the follow-up treatment strategy. Additionally, CEUS offers promising pathways for basic research on NR and myocardial infarction, enabling the safe and cost-effective evaluation of pharmacological treatments and providing valuable insights into different strategies' effectiveness.

Conclusion

We have successfully demonstrated the feasibility of using HFR CEUS as a reliable method for assessing coronary flow, or its absence, in a dedicated animal model with a temporarily occluded coronary artery and a contrast-destruction-reperfusion echo protocol. One of the significant aspects of this technique is its ability to distinguish between slow and fast flow, as well as flow direction in larger vessels, which may provide further clinically relevant insights into pre-arteriole and arteriole flow, as well as insights into arterial and venous flow. Use of the HOSVD scheme to process data from contrast-specific pulses allowed the detection of slow or even virtually stationary contrast agent as well as mild tissue motion, which would otherwise provide strong tissue motion artifacts in conventional detection schemes [23]. The ability to evaluate the entire microcirculatory flow could increase the reliability of myocardial perfusion assessments compared with current clinical contrast-enhanced echocardiography techniques that depict contrast agent presence only and not also flow.

Conflict of interest

There is no conflict of interest.

Acknowledgments

This work was part of the research program "Vernieuwingsimpuls – Vidi 2017" with project number QUANTO-16572, which is (partly) financed by the Dutch Research Council (NWO).

Data availability

The data are available upon reasonable request to the corresponding author.

Supplementary materials

Supplementary material associated with this article can be found in the online version at doi:10.1016/j.ultrasmedbio.2024.12.002.

References

[1] Vogel B, Claessen BE, Arnold SV, Chan D, Cohen DJ, Giannitsis E, et al. ST-segment elevation myocardial infarction. Nat Rev Dis Primers 2019;5(1):20. doi: 10.1038/s41572-019-0090-3.

[2] Ibanez B, James S, Agewall S, Antunes MJ, Bucciarelli-Ducci C, Bueno H, et al. 2017 ESC Guidelines for the management of acute myocardial infarction in patients presenting with ST-segment elevation: The Task Force for the management of acute myocardial infarction in patients presenting with ST-segment elevation of the European Society. Eur Heart J 2018;39(2):119–77. doi: 10.1093/eurheartj/ehx393.

[3] Bouleti C, Mewton N, Germain S. The no-reflow phenomenon: State of the art. Arch Cardiovasc Dis 2015;108(12):661–74. doi: 10.1016/j.acvd.2015.09.006.

[4] Niccoli G, Cosentino N, Spaziani C, Fracassi F, Tarantini G, Crea F. No-reflow: Incidence and detection in the cath-lab. Curr Pharm Des 2013;19(25):4564–75. doi: 10.1016/j.acvd.2015.09.006.

[5] Ndrepepa G, Tiroch K, Fusaro M, Keta D, Seyfarth M, et al. 5-year prognostic value of no-reflow phenomenon after percutaneous coronary intervention in patients with acute myocardial infarction. J Am Coll Cardiol 2010;55(21):2383–9. doi: 10.1016/j.jacc.2009.12.054.

[6] Resnic FS, Wainstein M, Lee MK, Behrendt D, Ohno-Machado L, Kirshenbaum JM, et al. No-reflow is an independent predictor of death and myocardial infarction after percutaneous coronary intervention. Am Heart J 2003;145(1):42–6. doi: 10.1067/mhj.2003.36.

[7] Van Kranenburg M, Magro M, Thiele H, de Waha S, Seyfarth M, Piek JJ, et al. Prognostic value of microvascular obstruction and infarct size, as measured by CMR in STEMI patients. JACC Cardiovasc Imaging 2014;7(9):930–9. doi: 10.1016/j.jcmg.2014.05.010.

[8] Camici PG, D'Amati G, Rimoldi O. Coronary microvascular dysfunction: Mechanisms and functional assessment. Nat Rev Cardiol 2015;12(1):48–62. doi: 10.1038/nrcardio.2014.160.

[9] Johnson PC. Overview of the microcirculation. Microcirculation 2008:xi–xxiv. doi: 10.1016/B978-0-12-374530-9.00022-X.

[10] Padro T, Manfrini O, Bugiardini R, Canty J, Cenko E, De Luca G, et al. ESC Working Group on Coronary Pathophysiology and Microcirculation position paper on "coronary microvascular dysfunction in cardiovascular disease.". Cardiovasc Res 2020;116(4):741–55. doi: 10.1093/cvr/cvaa003.

[11] Rezkalla SH, Stankowski RV, Hanna J, Kloner RA. Management of no-reflow phenomenon in the catheterization laboratory. JACC Cardiovasc Interv 2017;10(3):215–23. doi: 10.1016/j.jcin.2016.11.059.

[12] Dewey M, Siegel MJ, Willmann JK, Messroghli DR, Higgins CB. Clinical quantitative cardiac imaging for the assessment of myocardial ischaemia. Nat Rev Cardiol 2020;17(7):427–50. doi: 10.1038/s41569-020-0341-8.

[13] Martino F, Amici G, Rosner M, Ronco C, Novara G. Gadolinium-based contrast media nephrotoxicity in kidney impairment: The physio-pathological conditions for the perfect murder. J Clin Med 2021;10(2):1–15. doi: 10.3390/jcm10020271.

[14] Senior R, Becher H, Monaghan M, Agati L, Zamorano JL, Vanoverschelde JL, et al. Clinical practice of contrast echocardiography: Recommendation by the European Association of Cardiovascular Imaging (EACVI) 2017. Eur Heart J Cardiovasc Imaging 2017;18(11):1205. doi: 10.1093/ehjci/jex182.

[15] Vervliet N, Debals O, Sorber L, Van Barel M, De Lathauwer L. Tensorlab 3.0, http://www.tensorlab.net; 2016. Accessed January 3, 2025.

[16] Maresca D, Correia M, Villemain O, Bizé A, Sambin L, Tanter M, et al. Noninvasive imaging of the coronary vasculature using ultrafast ultrasound. JACC Cardiovasc Imaging 2018;11(6):798–808. doi: 10.1016/j.jcmg.2017.05.021.

[17] Demené C, Deffieux T, Pernot M, Osmanski BF, Biran V, Gennisson JL. Spatiotemporal clutter filtering of ultrafast ultrasound data highly increases Doppler and fUltrasound sensitivity. IEEE Trans Med Imaging 2015;34(11):2271–85. doi: 10.1109/TMI.2015.2428634.

[18] Demeulenaere O, Sandoval Z, Mateo P, Dizeux A, Villemain O, Gallet R, et al. Coronary flow assessment using 3-dimensional ultrafast ultrasound localization microscopy. JACC Cardiovasc Imaging 2022;15(7):1193–208. doi: 10.1016/j.jcmg.2022.02.008.

[19] Toulemonde M, Li Y, Lin S, Cordonnier F, Butler M, Duncan WC, et al. High-frame-rate contrast echocardiography using diverging waves: Initial in vitro and in vivo evaluation. IEEE Trans Ultrason Ferroelectr Freq Control 2018;65(12):2212–21. doi: 10.1109/TUFFC.2018.2856756.

[20] Toulemonde MEG, Corbett R, Papadopoulou V, Chahal N, Li Y, Leow CH, et al. High frame-rate contrast echocardiography: In-human demonstration. JACC Cardiovasc Imaging 2018;11(6):923–4. doi: 10.1016/j.jcmg.2017.09.011.

[21] Yan J, Huang B, Tonko J, Toulemonde M, Hansen-Shearer J, Tan Q, et al. Transthoracic ultrasound localization microscopy of myocardial vasculature in patients. Nat Biomed Eng 2024;8(6):689–700. doi: 10.1038/s41551-024-01206-6.

[22] De Lathauwer L, De Moor B, Vandewalle J. A multilinear singular value decomposition. SIAM J Matrix Anal Appl 2000;21(4):1253–78. doi: 10.1137/S0895479896305696.

[23] Wahyulaksana G, Wei L, Voorneveld J, Hekkert MTL, Strachinaru M, Duncker DJ, et al. Higher-order singular value decomposition filter for contrast echocardiography. IEEE Trans Ultrason Ferroelectr Freq Control 2023 Sep;70(11):1371–83. doi: 10.1109/tuffc.2023.3316130.

[24] Jensen JA. Estimation of blood velocities using ultrasound: A signal processing approach. Cambridge, UK: Cambridge University Press; 1996.

[25] Papadacci C, Pernot M, Couade M, Fink M, Tanter M. High-contrast ultrafast imaging of the heart. IEEE Trans Ultrason Ferroelectr Freq Control 2014;61(2):288–301. doi: 10.1109/TUFFC.2014.6722614.

[26] Rodriguez-Molares A, Repetto G, Løvstakken L. The UltraSound ToolBox. In: Paper presented at: IEEE International Ultrasonics Symposium; September, 6–9; 2017. doi: 10.1109/ULTSYM.2017.8092389.

[27] Duncker DJ, Canty Jr. JM. Coronary blood flow reserve and myocardial ischemia. Nuclear Cardiology: Basic and Advanced Concepts in Clinical Practice. Switzerland, AG: Springer Nature; 2021. p. 225–45.

[28] Spiller P, Schmiel FK, Pölitz B, Block M, Fermor U, Hackbarth W, et al. Measurement of systolic and diastolic flow rates in the coronary artery system by X-ray densitometry. Circulation 1983;68(2 Pt 1):337–47. doi: 10.1161/01.CIR.68.2.337.

[29] Feingold S, Gessner R, Guracar IM, Dayton PA. Quantitative volumetric perfusion mapping of the microvasculature using contrast ultrasound. Invest Radiol 2010;45(10):669–74. doi: 10.1097/RLI.0b013e3181ef0a78.

[30] Stanziola A, Toulemonde M, Li Y, Papadopoulou V, Corbett R, Duncan N, et al. Motion artifacts and correction in multi-pulse high-frame-rate contrast-enhanced ultrasound. IEEE Trans Ultrason Ferroelectr Freq Control 2018;66(2). doi: 10.1109/TUFFC.2018.2887164.